THERMOGRAVIMETRIC STUDY OF THE DECOMPOSITION OF PRINTED CIRCUIT BOARDS FROM MOBILE PHONES

Nuria Ortuño, Julia Moltó, Silvia Egea, Rafael Font & Juan A. Conesa

Chemical Engineering Department. University of Alicante. P.O. Box 99, 03080 Alicante (Spain). Phone: + (34) 96 590 38 67 Fax: + (34) 96 590 38 26

Author email address: nuria.ortuno@ua.es

ABSTRACT

Thermal decomposition of printed circuits boards (PCB) is studied, using thermogravimetric analysis to compare the thermal behavior of PCB of mobile phones before and after the removal of the metallic fraction by acid washing. Several dynamic and dynamic+isothermal runs have been carried out at different heating rates (5, 10 and 20 K/min), from room temperature to more than 1100 K. Also runs in the presence and in the absence of oxygen were performed (combustion and pyrolysis runs).

Moreover, TG-MS experiments were performed (both in inert and oxidizing atmosphere) in order to better understand the thermal decomposition of these wastes and identify some compounds emitted during the controlled heating of these materials.

Different reaction models are proposed, one for pyrolysis and one for combustion of the two kinds of wastes studied, which proved to simulate appropriately the experimental results at all the heating rates simultaneously.

KEYWORDS: Pyrolysis, combustion, kinetics, thermogravimetry, printed circuit board.

1. INTRODUCTION

The production of electrical and electronic equipment (EEE) is one of the fastest-growing sectors of the manufacturing industry in the world. At the same time, technological innovation and intense marketing engender a rapid replacement process. Every year, 20–50 million tonnes of waste electrical and electronic equipment (WEEE) are generated worldwide, which could bring serious risks to the human health and the

29　environment [UNEP, E-waste, the hidden side of IT equipment's manufacturing and use
30　E-waste, the hidden side of IT equipment's manufacturing and use, Environment Alert
31　Bulletin, 2005].

32　The Electrical and Electronic Equipment Waste Directive [1] promotes the re-use,
33　recycling and recovery of such electrical and electronic waste. The Directive requires
34　the separate collection of electrical and electronic waste as a separate waste stream,
35　which enhances the prospects for economic recycling.

36　Among these wastes, printed circuit boards are particularly problematic to recycle
37　because of the heterogeneous mix of organic material, metals, and glass fibre [2] and
38　low recycling rates are reported of about 15 % [3]. It has been estimated that PCB
39　comprise approximately 6 wt % of all WEEE, representing over 500,000 tonnes of
40　printed circuit boards generated in the EU27 per year [Das 09 RCR].

41　The metals present in PCB include large amounts of copper, aluminum and iron, and
42　also precious metals such as gold, silver and palladium, which increase the interest in
43　recycling technologies to recover such metals. In addition, the plastic fraction of the
44　PCB represents an important fraction to meet recycling and recovery targets set out in
45　the WEEE Directive [4]. In the past, the non metallic fractions were treated by
46　combustion, which can lead to the formation of toxic brominated compounds derived
47　from the brominated flame retardants contained in the circuit boards, or sent to landfill,
48　which can lead to toxic compounds leaching to the groundwater [5,6].

49　Thermogravimetric (TG) analysis is one of the techniques for studying the primary
50　reaction in the decomposition of solids and has been widely used to study the thermal
51　decomposition of PCB waste. The interpretation of the experimental data can provide
52　information on the composition of the sample, order of reaction, number of different
53　processes taking place in the reaction, and the corresponding kinetic constants [7].

54　Only a few authors proposed kinetic models that simulate the behavior of the thermal
55　degradation of the materials studied. Chien et. al. [8] studied the thermal decomposition
56　of waste printed circuit board using a fixed bed reactor with nitrogen at temperatures of
57　350 – 800 ºC and thermogravimetric analysis at a heating rate of 5 ºC min^{-1}. Kowalska
58　et al. [9] used TG analysis to study the pyrolysis of a heterogeneous mixture of printed
59　circuit boards (epoxy resin based) obtained from WEEE. Chiang et al. [10] investigated
60　the influence of particle size and process temperature on the pyrolysis of mixed waste

printed circuit boards collected from a recycling plant; pyrolysis was carried out in a laboratory scale quartz tube furnace between 200 and 500 ºC in nitrogen and they also undertook thermogravimetric analysis of the circuit boards to produce pyrolysis kinetic data in relation to sample heating rate. Li et. al. [11] conducted a thermo-analytical and kinetics study on PCBs by TG analysis under various atmospheres and focused on low-temperature scope. Barontini et al. [12] investigated the thermal degradation patterns of the plastic fraction of flame retarded epoxy resin after the removal of metal content, using a thermogravimetric analyser and a laboratory scale pyrolysis reactor; a simplified kinetic analysis was undertaken which considered a single-step first-order autocatalytic kinetic model.

Other authors [5,13-15] studied the pyrolysis of printed circuit boards from different e-wastes, at temperatures ranging from 300 to 800 ºC, and determined the corresponding solid, liquid and gas yields. Finally, some papers addressed the study of the thermal decomposition products of metal free flame retarded epoxy resins [7,16-20].

In a previous study [21], the thermal decomposition of used PCB from mobile phones was studied. The present work uses thermogravimetric analysis to compare the thermal behavior of PCB from mobile phones before and after the removal of the metallic fraction both in the presence and in the absence of oxygen, studies the main gaseous evolved products and proposes a kinetic model for the decomposition of each material.

2. EXPERIMENTAL

2.1. RAW MATERIAL

Two different materials were compared in the present study. On the one hand, waste printed circuit boards from mobile phones were separated and crushed to fine dust (sample named "PCB") using a vibratory disc mill by Herzog, HSM 100 (Osnabrüch, Germany). On the other hand, in order to remove the metallic fraction, a part of the sample was treated with a dilute aqueous solution of HCl and H_2O_2, followed by washing with deionized water and drying at 110 ºC (sample named "non metallic PCB").

Table 1 shows the ultimate analysis of both samples, obtained with a CHNS analyzer (FlashEA 1112 Series, ThermoFinnigan), whereas Table 2 shows the semi-quantitative analysis of the remaining elements, performed by X-ray fluorescence with an automatic sequential spectrometer (model TW 1480, PHILIPS MAGIX PRO, Philips Co., Ltd.).

93   For PCB, copper represents 24.19 wt % (weight percentage), whereas for non metallic

94   samples copper accounts only for 0.50 wt %, confirming the effectiveness of the acid

95   washing treatment. Other metals, such as Ca, Al, Pb, Sn, Ni or Fe, present also lower

96   values in the non metallic PCB sample. Consequently, other elements, as is the case of

97   Si or halogens, show an increase in their concentration in this washed sample.

98   <mark>Tables 1 and 2</mark>

99   2.2. THERMOBALANCE

100   The experiments of thermogravimetry were performed in a Mettler Toledo

101   thermobalance (model TGA/SDTA851e/LF/1600) with a horizontal furnace and a

102   parallel-guided balance. The position of the sample does not change during the

103   measurement, and flow gas perturbation and thermal buoyancy are minimized. The

104   sample temperature was measured with a sensor directly attached to the sample holder.

105   Good performance of the TG system was checked by carrying out one experiment with

106   Avicel PH-105 microcrystalline cellulose at 5 K min^{-1} in nitrogen and calculating the

107   corresponding kinetic constants of its thermal degradation, which were in good

108   agreement with those obtained in a roundrobin study of Avicel cellulose pyrolysis [22].

109   Pyrolysis (N_2) and combustion runs, N_2:O_2.= 4:1 (normal conditions) and N_2:O_2 = 9:1

110   (poor oxygen conditions), were carried out with a flow rate of 100 mL min^{-1}. Dynamic

111   experiments were carried out at three different heating rates (5, 10 and 20 K min^{-1}), from

112   room temperature to a final temperature higher than 1000 K, covering in this way an

113   extensive range of decomposition. Isothermal experiments started with a constant

114   heating rate until the set temperature was reached, and then the final temperature was

115   maintained constant throughout the pyrolysis or combustion process for, at least, 120

116   minutes; these final temperatures were selected according to the temperatures with the

117   highest weight loss in dynamic runs. The sample mass used was around 5 mg in all

118   cases, and under these conditions, it has been tested that the heat transfer effects are

119   very small.

120   The TG-MS runs were carried out in the same thermobalance coupled to a Pfeiffer

121   Vacuum mass spectrometer (model Thermostar GSD301T) to monitor the signal of the

122   volatile compounds evolved. Operating conditions for these experiments were as

123   follows: sample mass around 10 mg, heating rate 30 K min^{-1}, ionization 70 eV, SIR

124   mode, atmospheres of He and He:O_2 = 4:1. The response of the different ions was

125   normalized to that of helium (m/z = 4) and the minimum value was subtracted from

126   each one to relate all the values to zero.

127   3. RESULTS AND DISCUSSION

128   3.1. PRINTED CIRCUIT BOARDS ("PCB" SAMPLE)

129   3.1.1. THERMOGRAVIMETRIC STUDY

130   In order to study thermal decomposition of printed circuit boards ("PCB" sample),

131   several pyrolysis and combustion runs have been carried out in dynamic mode (constant

132   heating rate) or isothermal mode (constant heating rate until the set temperature is

133   reached and then constant temperature). Figure 1 shows the results in the presence of

134   nitrogen (pyrolysis runs). Figures 2 and 3 are the corresponding to 20 and 10 % of

135   oxygen respectively. In the figures, the weight fraction (on the left Y axis) represents

136   the residual mass fraction of the solid, i.e., the sum of the residue formed and the non-

137   reacted solid.

138   Figure 1A shows the TG plots for pyrolysis at three heating rates: 5, 10 and 20 K min^{-1}.

139   For the 20 K min^{-1} run, Figure 1A also shows the ΔT corresponding to the differential

140   thermal analysis (DTA). ΔT value is shown on the right Y-axis, and it is plotted in a

141   convenient scale, from -10 K for a strong endothermic process to $+10$ K corresponding

142   to a strong exothermic process. It can be concluded that there is neither a great heat

143   release nor consumption in these runs.

144   Figure 1B shows TG and derivative thermogravimetric analysis (DTG) curves for the

145   pyrolysis run at 20 K min^{-1}. It can be observed that there is an initial large peak (with

146   the maximum decomposition rate at 630 K) followed by a small band or wide peak

147   (from 680 to 800 K), which means that at least two fractions must be considered in the

148   decomposition, with a final residue of around 76 % of initial sample weight.

149   Three isothermal runs were carried out in pyrolytic conditions (Figure 1C). These

150   experiments started with constant heating rate until the desired temperature was

151   reached, and then the final temperature was maintained throughout the pyrolysis

152   process.

153   Figure 1

154   Figure 2A shows the experimental TG plots of combustion runs ($N_2:O_2 = 4:1$) at three

155   heating rates (5, 10, 20 K min^{-1}). The ΔT corresponding to the differential thermal

156 analysis (DTA) is also plotted for the run at 20 K min^{-1}. It can be observed that a small

157 exothermic band due to oxidative pyrolysis appears, and later a significant exothermic

158 process takes place in the last part of the decomposition due to strong oxidation.

159 Figure 2B shows TG and DTG runs for the combustion at 10 K min^{-1}. From the DTG

160 curve, it can be observed that there is an initial large peak, with the maximum

161 decomposition rate at 630 K that coincides with the first process observed in pyrolysis.

162 This is followed by a second peak at around 665 K followed by a decreasing peak at

163 770 K that stands for the oxidation of the metallic fraction. Lastly, a third increasing

164 peak is observed with maximum decomposition rate at 800 K, leading to a solid residue

165 yield of 85 wt %. The decomposition of the complete printed circuit board takes place

166 in three different processes, suggesting that at least three fractions must be considered in

167 the decomposition, apart from the oxidizing step.

168 The results of isothermal runs in a 4:1 N_2:O_2 atmosphere and at different heating rates

169 are shown in Figure 2C.

170   Figure 2

171 Figure 3A and 3B show the experimental results for dynamic and isothermal runs in a

172 9:1 N_2:O_2 atmosphere, with similar behavior to that observed with 4:1 N_2:O_2

173 atmosphere.

174   Figure 3

175 The main decomposition range of the residues studied in this paper is 570 − 750 K and

176 coincides with the previously reported by Moltó et. al. [21].

177 Comparing the results with other studies, the thermogravimetric analysis conducted by

178 Kowalska et al. [9] on the pyrolysis of three types of printed circuit boards indicated a

179 solid residue yield of ~74 wt % and two maxima of DTG at 593 and 629 K were

180 observed, but these two peaks were caused not only by dissimilar resins, being part of

181 both samples (epoxy resin and polyester resin) but also by different flame retardants

182 used as components. The results showed that the decomposition took place mainly in

183 the range 573 − 673 K, and at temperatures above 673 K, there was a slow

184 decomposition.

185 Hall and Williams [5] presented a TG pyrolysis run of mixed waste electrical and
186 electronic equipment. In this case the decomposition took place in the range 673 – 823
187 K, a little wider than that of the residues considered in the present paper.

188 According to Li et. al. [11], PCB degradation in air is clearly divided into three steps: in
189 step one (< 570 K), mass loss was restricted to a minimum level; in step two (570 - 673
190 K), the flame retardant decomposed and the gas or liquid products were released and in
191 step three (> 673 K), the TG curve returned to a smooth decrease, because a large
192 amount of the organic material was decomposed into gas and liquid products. These
193 stages coincide with the ones observed in the present study, although the weight gain
194 peak is not observed because these authors only carried out experiments up to 673 K,
195 delimiting the beginning of the metallic fraction oxidation.

196 3.1.2. STUDY OF THE EMISSIONS BY TG-MS

197 Different TG-MS run were carried out analyzing the evolution of the most relevant ions
198 in two atmospheres (He and He:O_2 = 4:1). All the runs were performed from room
199 temperature to more than 1000 K, at a heating rate of 30 K min^{-1}. The results were
200 carefully evaluated to determine the majority evolving compounds (considering the
201 relative abundances of the different fragments of each compound), since different ionic
202 species with the same m/z ratio can be easily mistaken. The evolution of some masses
203 corresponding to brominated compounds was followed but any of them was detected,
204 because the sensitivity of the mass spectrometer employed decreased rapidly for ions
205 with high m/z values.

206 Figure 4A shows the variation of ions 18, 28 and 44 of a pyrolysis run, corresponding to
207 water, CO and CO_2, which are the main gaseous products. Figure 4B shows the
208 response of ions with m/z equal to 16 (methane), 27 (ethylene), 41 (propylene) and 94
209 (phenol) in the same atmosphere. At a heating rate of 30 K min^{-1}, those compounds are
210 mostly emitted around 610 K, although methane is also emitted at around 800 K, thus
211 confirming that there are at least two fractions with different reactivity under pyrolytic
212 conditions.

213 For the runs carried out under oxidizing atmosphere (He:O_2 = 4:1), Figure 4C shows
214 that the main gaseous products are the same as in pyrolysis: water (m/z 18), CO (m/z
215 28) and CO_2 (m/z 44), but in that case three stages are observed during the evolution of
216 CO and CO_2 (at around 620, 690 and 800 K), whereas water is emitted in a wide range

217 of temperatures (500 – 800 K). Those peaks indicate that in addition to the two fractions
218 deduced in the pyrolysis, there are two more fractions, corresponding to an intermediate
219 oxidation or "oxidative pyrolysis" (second peak) and the oxidation of the metallic
220 fraction, that leads to an increase in weight. Apart from that, only ethylene is detected
221 (Figure 4D) at around 600 K, indicating that compounds such as methane, propylene
222 and phenol have been oxidized.

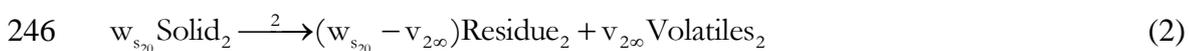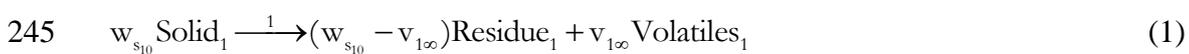223   Figure 4

224 With a comparison on literature sources subjected to N_2 or air atmosphere, while the
225 products released during the first phase were mainly H_2O and CO_2, the flame retardants
226 and other plastic additives were decomposed or volatilized, releasing small-molecule
227 products within the second phase, including HBr, H_2O, CO_2 and molecular
228 hydrocarbons (methane, ethane, and butane). Gases and liquid substances were released
229 from resin decomposition during the third phase; indicating that complete pyrolysis and
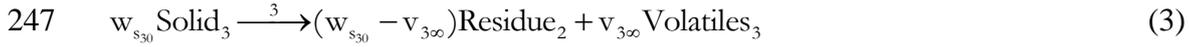230 carbonization occurred [11].

231 3.1.3. KINETIC MODEL

232 Different kinetic models were applied in order to simultaneously fit all TG curves under
233 dynamic and isothermal conditions. The range of temperatures used for the kinetic
234 calculation has been the complete range of decomposition, i.e., 350-1000 K. Above this
235 temperature, there are no other processes.

236 In a previous work by Molto et al. [21] a complex kinetic model was presented for the
237 thermal decomposition of PCB from mobile phones, in similar conditions to the ones
238 applied in the present study. The model presented was not able to reproduce the increase
239 of the weigth due to the oxidation of the metallic fraction of the sample. In the present
240 work the model has been significantly simplified, and, as will be shown later, it will be
241 able to explain the increase in the weight.

242 The kinetic model proposed for the pyrolysis of PCB could be interpreted considering
243 the material formed by three independent parts, each one following an independent
244 reaction, as follows:

245 $$w_{s_{10}}\text{Solid}_1 \xrightarrow{\;\;1\;\;} (w_{s_{10}} - v_{1\infty})\text{Residue}_1 + v_{1\infty}\text{Volatiles}_1 \tag{1}$$

246 $$w_{s_{20}}\text{Solid}_2 \xrightarrow{\;\;2\;\;} (w_{s_{20}} - v_{2\infty})\text{Residue}_2 + v_{2\infty}\text{Volatiles}_2 \tag{2}$$

247 $\quad w_{s_{30}} \text{Solid}_3 \xrightarrow{\ 3\ } (w_{s_{30}} - v_{3\infty})\text{Residue}_2 + v_{3\infty}\text{Volatiles}_3$ (3)

248 Solid$_i$ refers to the different fractions of the original material (i = 1 to 3), Volatiles$_i$ are

249 the gases and volatiles evolved in the corresponding reactions, and Residue$_i$ is the

250 possible residue formed in the decomposition of each Solid$_i$. Lower case letters

251 represent the yield coefficients representative of each reaction and, consequently, it is

252 considered that they do not change with time or with the extension of the reaction. Each

253 fraction has a yield coefficient that represents the maximum mass fraction obtainable by

254 each reaction. In this way, $v_{i\infty}$ is the yield coefficient for the Volatiles$_i$ that coincides

255 with the maximum mass fraction of volatiles that can be evolved at infinite time.

256 The conversion degree for each reaction is defined as the ratio between the mass

257 fraction of solid reacted at any time ($w_{si0} - w_{si}$) and the corresponding initial fraction of

258 this component w_{si0}, or the ratio between the mass fraction of volatiles obtained at any

259 time during which the reaction is taking place V_i and the corresponding yield coefficient

260 $v_{i\infty}$, so:

261 $\quad \alpha_i = \dfrac{w_{s_{i0}} - w_{s_i}}{w_{s_{i0}}} = \dfrac{V_i}{v_{i\infty}} \quad$ for i = 1 to 3 (4)

262 where w_{si0} is the weight fraction of each Solid$_i$ in the original material, and

263 consequently:

264 $\quad \displaystyle\sum_{i=0}^{3} w_{s_{i0}} = 1$ (5)

265 From the mass balance between products and reactants and the conversion degrees, the

266 kinetic equations for the pyrolysis runs can be expressed as follow:

267 $\quad -\dfrac{d\left(\dfrac{w_{s_i}}{w_{s_{i0}}}\right)}{dt} = \dfrac{d\left(\dfrac{V_i}{v_{i\infty}}\right)}{dt} = \dfrac{d\alpha_i}{dt} = k_i\left(\dfrac{w_{si}}{w_{s_{i0}}}\right)^{n_i} = k_i\left(1 - \alpha_i\right)^{n_i} = k_i\left[1 - \dfrac{V_i}{v_{i\infty}}\right]^{n_i}$ (6)

268 with the kinetic constants following the Arrhenius equation:

269 $\quad k_i = k_{i0}\exp\left(-\dfrac{E_i}{RT}\right) \quad$ for i = 1 to 3 (7)

270 By integration of these equations, it is possible to calculate α_i at each time if the

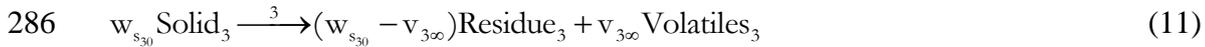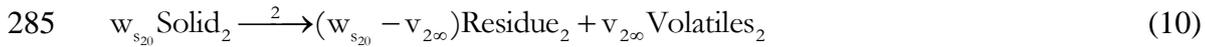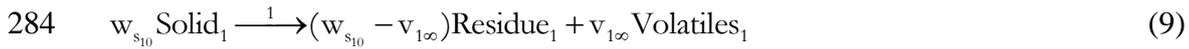271 temperature program T(t) is known. The relationship between α_i values and the weight

9

272 fraction measured in the thermobalance (w) is related with the total volatile fraction
273 obtained (V) by:

$$w = 1 - V = 1 - F_V \left(v_{1\infty}\alpha_1 + v_{2\infty}\alpha_2 + v_{3\infty}\alpha_3 \right) \tag{8}$$

275 In the previous equation, a correcting factor F_V has been introduced due to the fact that
276 the samples can have a slight but significant different content of inert material, due to
277 the heterogeneity of the samples studied. In all the cases the values F_V considered are
278 between 0.99 and 1.05.

279 For combustion reactions, the proposed scheme considers four initial solid fractions.
280 One of them accounts for the oxidation of metallic fractions, where the sample increases
281 its weight due to the formation of oxides and the other three fractions are equivalent to
282 those shown in pyrolytic conditions. The scheme proposed is the following one:

283 - Organic matter decomposition: three pyrolytic reactions:

$$w_{s_{10}}\text{Solid}_1 \xrightarrow{\;1\;} (w_{s_{10}} - v_{1\infty})\text{Residue}_1 + v_{1\infty}\text{Volatiles}_1 \tag{9}$$

$$w_{s_{20}}\text{Solid}_2 \xrightarrow{\;2\;} (w_{s_{20}} - v_{2\infty})\text{Residue}_2 + v_{2\infty}\text{Volatiles}_2 \tag{10}$$

$$w_{s_{30}}\text{Solid}_3 \xrightarrow{\;3\;} (w_{s_{30}} - v_{3\infty})\text{Residue}_3 + v_{3\infty}\text{Volatiles}_3 \tag{11}$$

287 - Metal oxidation: one fraction is considered where there is an increase of weight.

$$w_{s_{40}}\text{Solid}_4 + v_{4\infty}O_2 \xrightarrow{\;4\;} (w_{s_{40}} + v_{4\infty})\text{Residue}_4 \tag{12}$$

289 The kinetic equations, considering conversion degrees are the following:

$$\frac{d\alpha_i}{dt} = k_i \left(1 - \alpha_i \right)^{n_i} \quad \text{for } i = 1 \text{ to } 4 \tag{13}$$

291 The dependence of oxygen has been considered with the following expressions:

$$k_{i0}^* = k_{i0} \left[\frac{p_{O2}}{0.20} \right]^b \tag{14}$$

293 where the pre-exponential factor k_{i0} is directly proportional to the oxygen pressure, and
294 p_{O2} is the partial pressure of oxygen in atm. Logically, k_{i0}^* equals k_{i0} working with
295 $N_2:O_2 = 4:1$ atmosphere (p_{O2} equals 0.20 atm). The values of coefficient b have been
296 obtained for each reaction.

297　The total weight fraction (w) and the volatile weight fraction (V) are related with the
298　conversion degrees by:

$$w = 1 - V = 1 - F_P \left(v_{1\infty} \alpha_1 + v_{2\infty} \alpha_2 + v_{3\infty} \alpha_3 \right) + F_M \left(v_{4\infty} \alpha_4 \right) \qquad (15)$$

300　where $v_{i\infty}$ represent the maximum values in accordance with the scheme of reactions
301　proposed, and F_P and F_M are, respectively, weight factors corresponding to the
302　polymeric fraction that can decompose and to the metal fraction that can be oxidized. In
303　this case, this weight factors obtained also by optimization vary between 0.90 and 1.10.
304　It must be emphasized that these factors are included considering that each sample can
305　contain different quantities of fractions that can be decomposed or oxidized. In
306　duplicated runs, it has been tested that the volatile mass evolved at infinite time in TG
307　runs can be slightly different from one sample to another.

308　The correlation parameters were obtained by integration of the differential equations
309　presented in the kinetic model, with the Euler method, but considering and testing that
310　the intervals of time were small enough, so the errors introduced are negligible. The
311　optimization was done by using Solver function in an Excel spreadsheet, minimizing the
312　differences between experimental and calculated weight loss values and their
313　derivatives. The objective function to minimize was the sum of the square differences
314　between experimental and calculated total volatile V:

$$OF = \sum_{m=1}^{M} \sum_{j=1}^{N} (V_{m,j}^{exp} - V_{m,j}^{cal})^2 \qquad (16)$$

316　where M is the number of runs and N is the number of points in each run.

317　The model validity was tested calculating the variation coefficient (VC):

$$VC = \frac{\sqrt{\dfrac{OF}{N_{total} - P}}}{\overline{V_{exp}}} \cdot 100 \qquad (17)$$

319　where N_{total} and P are the number of data and parameters fitted, respectively, and $\overline{V_{exp}}$
320　is the average of the experimental values of weight fraction corresponding to the
321　volatiles evolved.

322　The kinetic parameters obtained are shown in Table 3. The calculated curves are shown
323　in Figures 1, 2 and 3, where the experimental data are also presented, overlapping the

324 experimental curves in most cases. The mean variation coefficient for the correlation of
325 all experimental data (dynamic and isothermal runs at different heating rates) by using
326 the same kinetic constants, and considering the weight fraction of volatiles evolved, is
327 1.4 % for pyrolysis and 5.4 % for combustion, which are relatively small values.

328 Table 3

329 Figure 5 shows the contribution of each reaction in the decomposition process. In
330 Figure 5A the mass fractions of the residues in the three pyrolytic processes are shown;
331 it can be observed that there are two main fractions (1 and 2). In Figure 5B,
332 corresponding to the combustion process, the residues corresponding to all reactions can
333 be observed, showing that all the reactions implied are important in the satisfactory
334 correlation of the data.

335 Figure 5

336 To obtain a single set of parameters for the pyrolysis and for the combustion kinetic
337 models for printed circuit boards, all the runs were correlated simultanously in order to
338 obtain only one set of parameters valid for any condition.

339 3.2. METAL FREE PRINTED CIRCUIT BOARDS ("NON METALLIC PCB"
340 SAMPLE)

341 3.2.1. THERMOGRAVIMETRIC STUDY

342 In order to compare the thermal behavior of printed circuit boards before and after metal
343 removal, the same set of pyrolysis and combustion runs were carried out with the "non
344 metallic PCB" sample. In summary, nine dynamic experiments were carried out by
345 combining three different atmospheres (N_2, N_2:O_2 = 9:1 and N_2:O_2 = 4:1) and three
346 heating rates (5, 10 and 20 K min^{-1}) from room temperature to more than 1100 K, and
347 other nine dynamic + isothermal runs were performed (same final temperatures as for
348 the PCB sample). Figures 6 to 8 show the experimental results.

349 Figure 6A shows the TG plots for pyrolysis at three heating rates: 5, 10 and 20 K min^{-1},
350 as well as the DTA increment of temperature for the 20 K min^{-1} run that shows that no
351 great heat release nor consumptions occurs in these runs. Figure 6B shows TG and DTG
352 curves for the pyrolysis run at 20 K min^{-1}. As for the PCB sample, an initial large peak
353 (with a maximum in DTG at 615 K) followed by a small band is observed (also from
354 680 to 800 K), that leads to a solid yield of 50 wt %; this suggests to consider at least

355 two fractions in the decomposition of the non metallic PCB sample. Figure 6C shows

356 the isothermal runs carried out in pyrolytic conditions at three different final

357 temperatures and initial heating rates.

358   Figure 6

359 Figure 7A shows the experimental TG plots of combustion runs ($N_2:O_2 = 4:1$) at 5, 10

360 and 20 K min^{-1} and the ΔT curve at 20 K min^{-1}. A wide exothermic peak is observed in

361 DTA analysis, formed by three consecutive smaller peaks that correspond to a strong

362 oxidation of the sample. Figure 7B shows TG and DTG curves for the combustion at 20

363 K min^{-1}. In oxygen presence, an initial large peak is observed at around 610 K in the

364 DTG run; as for the PCB sample, this peak coincides with the first process observed in

365 pyrolysis (Figure 6B). A little peak appears at 735 K and a third bigger DTG peak is

366 observed at 800 K, producing a final solid residue of about 39 wt %. In this way, these

367 observations confirm that the decomposition of the metal free circuit boards takes place

368 in three different processes. The isothermal runs at different heating rates in 4:1 $N_2:O_2$

369 atmosphere are shown in Figure 7C.

370   Figure 7

371 Figure 8 shows the experimental results for dynamic and isothermal runs in a 9:1 $N_2:O_2$

372 atmosphere, with similar behavior to that observed with 4:1 $N_2:O_2$ atmosphere.

373   Figure 8

374 The main decomposition temperature range observed for non metallic PCB in this work

375 is 570 – 750 K (as it happened for PCB sample). This range is a little wider, but still in

376 good agreement with the data reported in previous studies, which suggest that the

377 thermal degradation process of the organic components of electronic scrap at low

378 heating rates takes place at temperatures between 550 and 650 K [23-25].

379 For non metallic PCB, the first weight loss process starts at similar temperatures in inert

380 and oxidizing environments, indicating that this stage does not depend on the presence

381 of oxygen; however, a higher residue results from this decomposition step in the

382 presence of oxygen. A higher thermal stability in air at temperatures between 523 and

383 673 K was reported in the literature for several materials (e.g., diisocyanates,

384 polyurethanes, etc.), and was attributed to the occurrence of cross-linking and

385 condensation radical reactions during the thermal decomposition [12]. The second stage

386 occurs over a longer temperature range compared to the one in air due to decomposition

387 and release of various fragments over different temperature ranges [26]. On the other

388 hand, in air, some fragments begin to be oxidized whilst the resin is decomposing [18].

389 Biswas et. al. [18] also reported three stages in the degradation of pure epoxy uncured

390 resin in air at 10 K min^{-1}: a first stage due to water loss through curing and dehydration

391 (up to 538 K) with 10 % mass loss, a second stage due to the decomposition to a char

392 (623 − 733 K) with 30 % mass loss and a third stage corresponding to char oxidation

393 (713 − 893 K) with 57 % mass loss leaving 2.5 % char residue at the end. In nitrogen

394 atmosphere, only two stages were reported: a first stage (up to 538 K) with 8 % mass

395 loss and a second stage in the temperature range (632 − 795 K) with 62% mass loss

396 leaving 29.9 % char residue at 1173 K

397 3.1.2. STUDY OF THE EMISSIONS BY TG-MS

398 Experimental results of different TG-MS runs for the metal free sample (non metallic

399 PCB) are shown in Figure 9. Figure 9A shows the evolution of water (m/z 18), carbon

400 dioxide (m/z 44) and carbon monoxide (m/z 28) at around 600 K in pyrolysis. In Figure

401 9B, two peaks can be observed for the evolution of methane (m/z 16) and ethylene (m/z

402 27) at 600 and 800 K, whereas propylene (m/z 41) and phenol (m/z 94) are mostly

403 emitted at the low temperature peak.

404 Figure 9C and 9D shows the results for the runs carried out under oxidizing atmosphere

405 (He:O_2 4:1). Here, the main gaseous products are also water, CO and CO_2, but in

406 oxygen presence evolution of water (m/z 18) occurs in a wider temperature range,

407 between 470 and 900 K, with the highest emission rate at around 590 K, whereas CO

408 and CO_2, which are emitted along a similar temperature range, present a maximum at

409 around 780 K. Ethylene is detected (Figure 9D) at around 600 K, indicating that

410 compounds such as methane, propylene and phenol has been oxidized, as happened

411 with the PCB sample.

412   Figure 9

413 Barontini et al. [12,17] used TGA-FTIR and a small batch reactor to investigate the

414 pyrolysis of the plastic fraction of flame retarded epoxy resin, after the removal of

415 metals, and reported that the most prominent gas was HBr followed by CO_2 and CO;

416 only small amounts of CH_4 were reported. The evolution of CO and CO_2 was mainly

417 detected during the second step of the thermal degradation of electronic boards in air

418 (623 - 823 K). This confirms that this second weight loss step is mainly due to the

419 oxidation of the residual char formed at lower temperatures (during the main thermal
420 degradation process identified by the first weight loss step).

421 3.2.3. KINETIC MODEL

422 In this section, the same methodology and nomenclature is observed as for the PCB
423 sample (see Section 3.1.3).

424 Similarly to the one proposed for printed circuit boards, three fractions have been
425 considered in the pyrolysis kinetic model (see Eq. 1, 2 and 3).

426 For combustion, the scheme selected considers the same initial solid fractions and the
427 same reactions as the pyrolysis model. In this case, unlike the model for PCB samples,
428 no reaction considers the oxidation of metallic fractions, since this fraction has been
429 removed by acid washing. Furthermore, the TG curve in oxygen atmosphere does not
430 indicate an increase of the weight due to the formation of metal oxides, as was the case
431 for non washed PCB sample.

432 The total weight fraction (w) and the volatile weight fraction (V) are related with the
433 conversion degrees by Eq. (8), where the factor F_V ranges between 0.90 and 1.10 for all
434 runs.

435 The correlation parameters were obtained in the same way as for PCB and the results
436 are shown in Table 4. The calculated curves are also shown in Figures 6 to 8, together
437 with the experimental data. The mean variation coefficient for the correlation of
438 experimental data, considering the weight fraction of volatiles evolved is 1.7 % for the
439 pyrolytic model and 4.6 % for the combustion one, which indicate that correlations are
440 satisfactory.

441   Table 4

442 Figure 10 shows the contribution of each reaction in the decomposition process. In
443 Figure 10A the evolution of the residue mass fractions in the pyrolytic processes are
444 shown and, as in the PCB, reactions 1 and 2 are the most relevant. In Figure 10B, the
445 residues corresponding to each fraction in the combustion process are shown, where all
446 the reactions implied are important in the satisfactory correlation of the data.

447   Figure 10

448 Comparing results for PCB and non-metallic PCB samples, in pyrolysis runs, where
449 only the organic polymer decomposes, the final residue is approximately the same for

15

450 all the runs, although the residue from the non metallic sample is much lower (50 versus
451 76 wt %).

452 In the presence of oxygen, the PCB sample presents an oxidation of the metallic
453 compounds and this probably generates a different residue at infinite time. As proposed
454 by Moltó et. al. [21], the presence of metals and other compounds catalyzes the
455 decomposition of the organic matter. Also, an increase of weight is observed due to the
456 formation of metallic oxides that lately decompose. Support of this idea is found in the
457 behavior of the non metallic PCB sample, where no weight gain is observed.

458 4. CONCLUSIONS

459 The thermal behavior of printed circuit boards, before and after metal removal, has been
460 studied through thermogravimetric analysis under several different operating conditions
461 and the evolution of the main gaseous compounds has been analyzed by TG-MS.

462 Different kinetic models for the pyrolysis and combustion of these materials are
463 proposed, for which one set of parameters can explain many experiments under
464 different operating conditions. An acceptable correlation can be obtained for dynamic
465 runs at different heating rates and isothermal runs at distinct temperature operation.

466 ACKNOWLEDGMENTS

470

471   REFERENCES

472   [1]   E. Comission, in Official Journal of the European Comission, Brussels, 2003.
473   [2]   P. Williams, Valorization of Printed Circuit Boards from Waste Electrical and
474   Electronic Equipment by Pyrolysis, Waste and Biomass Valorization 1 (2010)
475   107-120.
476   [3]   M. Goosey, R. Kellner, in, Intellect and the Department of Trade and Industry,
477   London, 2002.
478   [4]   M. Schlummer, L. Gruber, A. Mäurer, G. Wolz, R. van Eldik, Characterisation
479   of polymer fractions from waste electrical and electronic equipment (WEEE)
480   and implications for waste management, Chemosphere 67 (2007) 1866-1876.
481   [5]   W.J. Hall, P.T. Williams, Separation and recovery of materials from scrap
482   printed circuit boards, Resources, Conservation and Recycling 51 (2007) 691-
483   709.
484   [6]   H. Li, L. Yu, G. Sheng, J. Fu, P.a. Peng, Severe PCDD/F and PBDD/F Pollution
485   in Air around an Electronic Waste Dismantling Area in China, Environ. Sci.
486   Technol. 41 (2007) 5641-5646.
487   [7]   C. Quan, A. Li, N. Gao, Thermogravimetric analysis and kinetic study on large
488   particles of printed circuit board wastes, Waste Management 29 (2009) 2353-
489   2360.
490   [8]   Y.-C. Chien, H. Paul Wang, K.-S. Lin, Y.J. Huang, Y.W. Yang, Fate of bromine
491   in pyrolysis of printed circuit board wastes, Chemosphere 40 (2000) 383-387.
492   [9]   E. Kowalska, J. Radomska, P. Konarski, R. Diduszko, J. Oszczudłowski, T.
493   Opalińska, M. Więch, Z. Duszyc, Thermogravimetric investigation of wastes
494   from electrical and electronic equipment (WEEE), J. Therm. Anal. Calorim. 86
495   (2006) 137-140.
496   [10]   H.-L. Chiang, K.-H. Lin, M.-H. Lai, T.-C. Chen, S.-Y. Ma, Pyrolysis
497   characteristics of integrated circuit boards at various particle sizes and
498   temperatures, J. Hazard. Mater. 149 (2007) 151-159.
499   [11]   J. Li, H. Duan, K. Yu, L. Liu, S. Wang, Characteristic of low-temperature
500   pyrolysis of printed circuit boards subjected to various atmosphere, Resources,
501   Conservation and Recycling 54 (2010) 810-815.
502   [12]   F. Barontini, K. Marsanich, L. Petarca, V. Cozzani, Thermal Degradation and
503   Decomposition Products of Electronic Boards Containing BFRs, Ind. Eng.
504   Chem. Res. 44 (2005) 4186-4199.
505   [13]   I. de Marco, B.M. Caballero, M.J. Chomón, M.F. Laresgoiti, A. Torres, G.
506   Fernández, S. Arnaiz, Pyrolysis of electrical and electronic wastes, J. Anal.
507   Appl. Pyrolysis 82 (2008) 179-183.
508   [14]   G. Jie, L. Ying-Shun, L. Mai-Xi, Product characterization of waste printed
509   circuit board by pyrolysis, J. Anal. Appl. Pyrolysis 83 (2008) 185-189.
510   [15]   C. Vasile, M.A. Brebu, M. Totolin, J. Yanik, T. Karayildirim, H. Darie,
511   Feedstock Recycling from the Printed Circuit Boards of Used Computers,
512   Energy Fuels 22 (2008) 1658-1665.
513   [16]   M.P. Luda, A.I. Balabanovich, G. Camino, Thermal decomposition of fire
514   retardant brominated epoxy resins, J. Anal. Appl. Pyrolysis 65 (2002) 25-40.
515   [17]   F. Barontini, V. Cozzani, Formation of hydrogen bromide and
516   organobrominated compounds in the thermal degradation of electronic boards, J.
517   Anal. Appl. Pyrolysis 77 (2006) 41-55.

518   [18]   B. Biswas, B.K. Kandola, A.R. Horrocks, D. Price, A quantitative study of
519   carbon monoxide and carbon dioxide evolution during thermal degradation of
520   flame retarded epoxy resins, Polym. Degrad. Stab. 92 (2007) 765-776.

521   [19]   M.P. Luda, A.I. Balabanovich, M. Zanetti, D. Guaratto, Thermal decomposition
522   of fire retardant brominated epoxy resins cured with different nitrogen
523   containing hardeners, Polym. Degrad. Stab. 92 (2007) 1088-1100.

524   [20]   G. Grause, M. Furusawa, A. Okuwaki, T. Yoshioka, Pyrolysis of
525   tetrabromobisphenol-A containing paper laminated printed circuit boards,
526   Chemosphere 71 (2008) 872-878.

527   [21]   J. Moltó, R. Font, A. Gálvez, J.A. Conesa, Pyrolysis and combustion of
528   electronic wastes, J. Anal. Appl. Pyrolysis 84 (2009) 68-78.

529   [22]   M. Grønli, M.J. Antal, G. Varhegyi, A Round-Robin Study of Cellulose
530   Pyrolysis Kinetics by Thermogravimetry, Ind. Eng. Chem. Res. 38 (1999) 2238-
531   2244.

532   [23]   M. Webb, P.M. Last, C. Breen, Synergic chemical analysis – the coupling of TG
533   with FTIR, MS and GC-MS: 1. The determination of the gases released during
534   the thermal oxidation of a printed circuit board, Thermochim. Acta 326 (1999)
535   151-158.

536   [24]   M. Blazsó, Z. Czégény, C. Csoma, Pyrolysis and debromination of flame
537   retarded polymers of electronic scrap studied by analytical pyrolysis, J. Anal.
538   Appl. Pyrolysis 64 (2002) 249-261.

539   [25]   C. Mazzocchia, A. Kaddouri, G. Modica, R. Nannicini, G. Audisio, C. Barbieri,
540   F. Bertini, Hardware components wastes pyrolysis: energy recovery and liquid
541   fraction valorisation, J. Anal. Appl. Pyrolysis 70 (2003) 263-276.

542   [26]   B.K. Kandola, A.R. Horrocks, P. Myler, D. Blair, in *Fire and Polymers*,
543   American Chemical Society, 2001, p. 344-360.

544

545

546   Table 1. Ultimate analysis of the materials used.

547

wt %	PCB	non metallic-PCB
C	20.4	36.4
H	1.9	3.4
N	0.7	1.4
S	nd	nd
O and ash (by difference)	77.0	58.7

nd: not detected

548

549

550   Table 2. Fluorescence analysis of the material used.

551

wt %	PCB	non metallic-PCB
O	24.49	21.73
Cu	24.19	0.50
Si	10.48	15.27
Br	5.67	12.16
Ca	4.52	3.78
Al	3.27	1.53
Pb	0.89	0.03
Sn	1.42	0.47
Ni	0.29	0.06
Ba	0.16	0.69
P	0.40	0.45
Fe	0.16	0.12
Ti	0.15	0.21
S	0.19	0.16
Cl	0.13	1.04
Ag	0.10	0.08
I	0.10	n.d.
Au	0.06	0.14
Zn	0.07	0.01
Mg	0.19	0.13
Sr	0.05	0.07
K	0.03	0.03
Cr	0.02	n.d.
Zr	0.03	0.04
Nb	0.01	n.d.
Nd	n.d.	0.05

nd: not detected

552

553

554   Table 3. Kinetic parameters obtained for the pyrolysis and combustion models of

555   printed circuit boards (PCB sample).

556

Reaction	$v_{i\infty}$	k_{io} (s^{-1})	E_i (kJ mol^{-1})	n_i	b (for O_2)
Pyrolysis					
1	0.120	$1.242 \cdot 10^{11}$	154.4	0.87	-
2	0.107	$2.600 \cdot 10^{23}$	300.2	8.00	-
3	0.124	0.2279	67.1	6.00	-
VC (%)	1.4				
Combustion					
1	0.080	$1.243 \cdot 10^{11}$	165.0	1.40	0.66
2	0.085	$2.600 \cdot 10^{23}$	272.3	4.76	0.66
3	0.110	$1.639 \cdot 10^{4}$	96.7	0.69	0.66
4	0.102	$4.401 \cdot 10^{4}$	98.2	0.41	0.72
VC (%)	5.4				

557

558

559   Table 4. Kinetic parameters obtained for the pyrolysis and combustion models of the

560   non-metallic fraction of printed circuit boards (non-metallic PCB sample).

561

Reaction	$v_{i\infty}$	k_{io} (s^{-1})	E_i (kJ mol^{-1})	n_i	b (for O_2)
Pyrolysis					
1	0.285	$7.418 \cdot 10^{12}$	170.5	1.15	-
2	0.208	$1.630 \cdot 10^{21}$	280.4	4.89	-
3	0.112	44.11	88.6	8.00	-
VC (%)	1.7				
Combustion					
1	0.250	$7.418 \cdot 10^{12}$	170.5	1.15	0.05
2	0.040	$1.630 \cdot 10^{21}$	280.4	4.89	0.05
3	0.330	$7.195 \cdot 10^{7}$	146.6	1.72	0.05
VC (%)	4.6				

562

563

564   Figure 1. Different pyrolysis runs of printed circuit boards: (A) Dynamic experimental
565   runs at three heating rates (the calculated curves overlap the experimental ones) and
566   DTA curve for the run at 20 K min^{-1}. (B) TG and DTG curves (experimental and
567   calculated) at 20 K min^{-1}. (C) Isothermal TG curves (experimental and calculated) at
568   different heating rates.

569

570

571
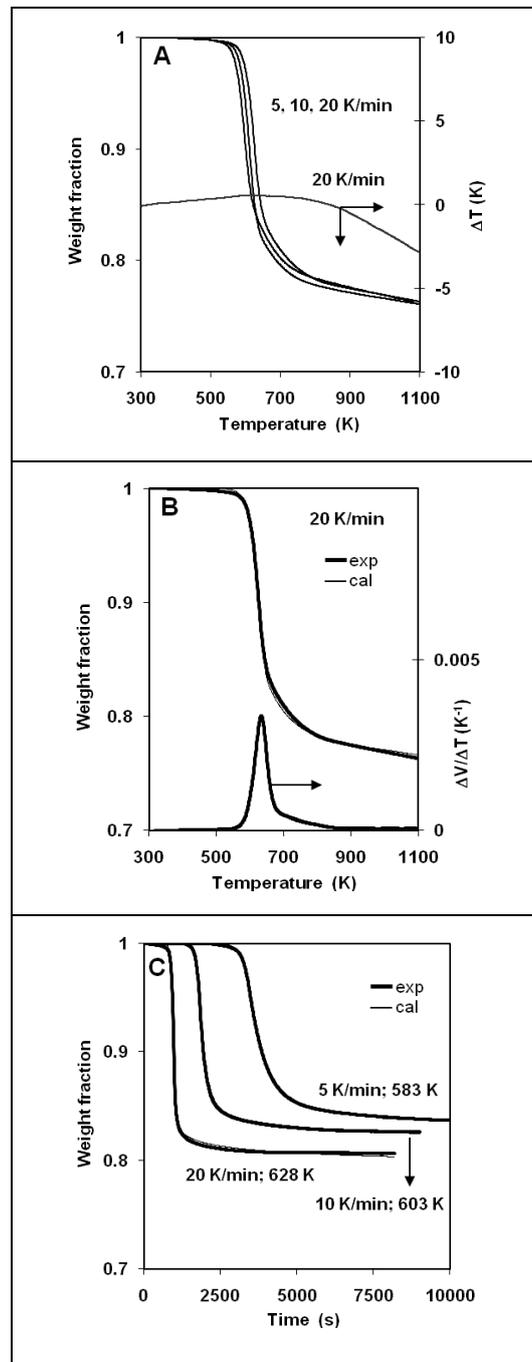
Figure 2. Different combustion (N_2:O_2 = 4:1) runs of printed circuit boards (experimental and calculated curves): (A) Dynamic TG curves at 5, 10 and 20 K min^{-1} and DTA curve for the run at 20 K min^{-1}. (B) TG and DTG curves at 10 K min^{-1}. (C) TG isothermal curves at different heating rates.

REVISAR FIGURAS DESDE AQUÍ
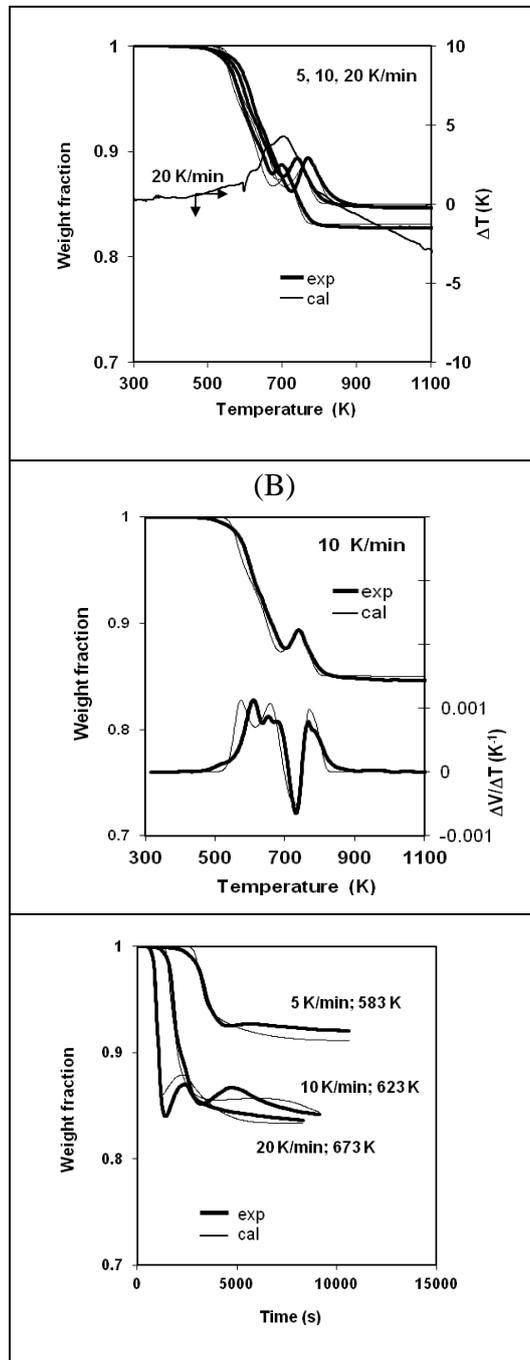
579   Figure 3. Different combustion ($N_2:O_2 = 9:1$) runs of printed circuit boards at 5, 10 and

580   20 K min^{-1} (experimental and calculated curves): (A) Dynamic TG runs. (B) Isothermal

581   TG runs.

582
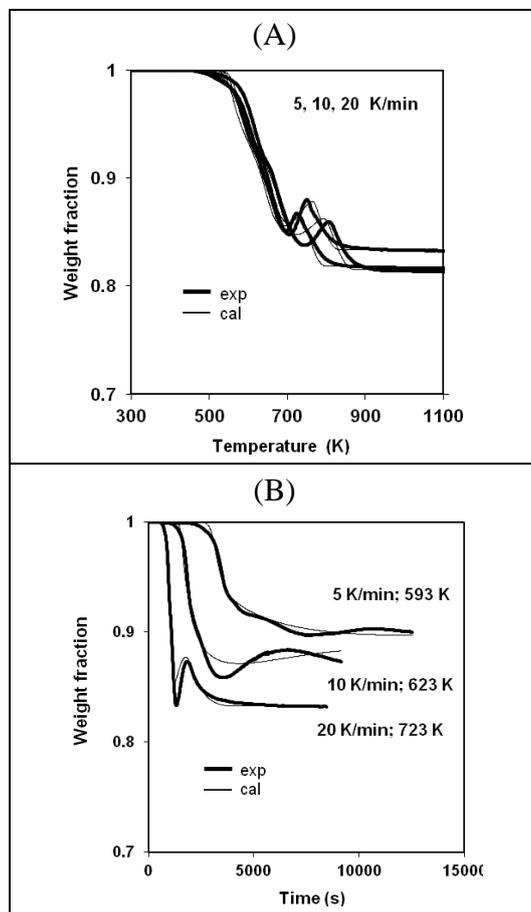
583

584

585　Figure 4. TG-MS of printed circuit boards at a heating rate of 30 K min^{-1}: (A) Intensity

586　of ions m/z 18 (water), 28 (CO) and 44 (CO_2) in pyrolysis (He). (B) Intensity of ions

587　m/z 16 (methane), 27 (ethylene), 41 (propylene) and 94 (phenol) in pyrolysis (He). (C)

588　and (D) Intensity of the same ions as (A) and (B) in combustion (He:O_2 4:1).

589
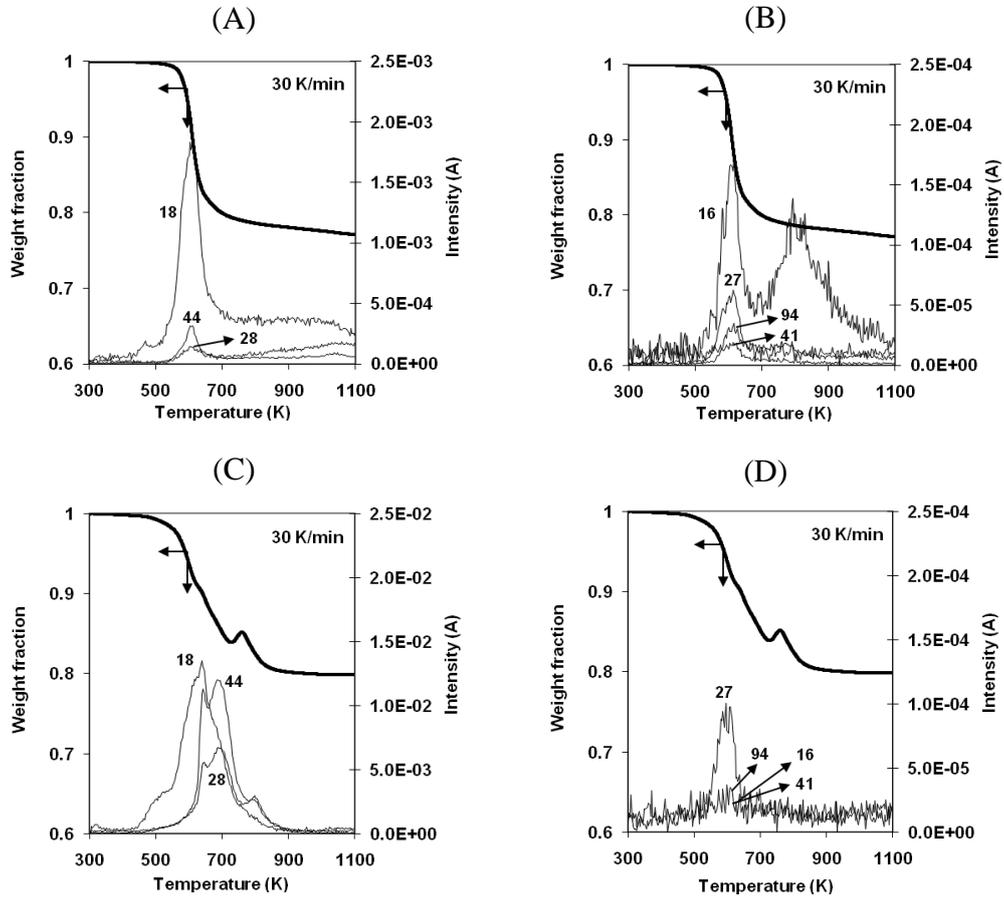
590

591

592 Figure 5. Evolution of the weight mass and the weight fraction of residues for each

593 reaction, PCB sample: (A) Pyrolysis TG run. (B) Combustion TG run (N_2:O_2 = 4:1

594 atmosphere).

595 <mark>CAMBIAR PARA QUE SE VEA COMO SUBE LA FRACCIÓN 4</mark>
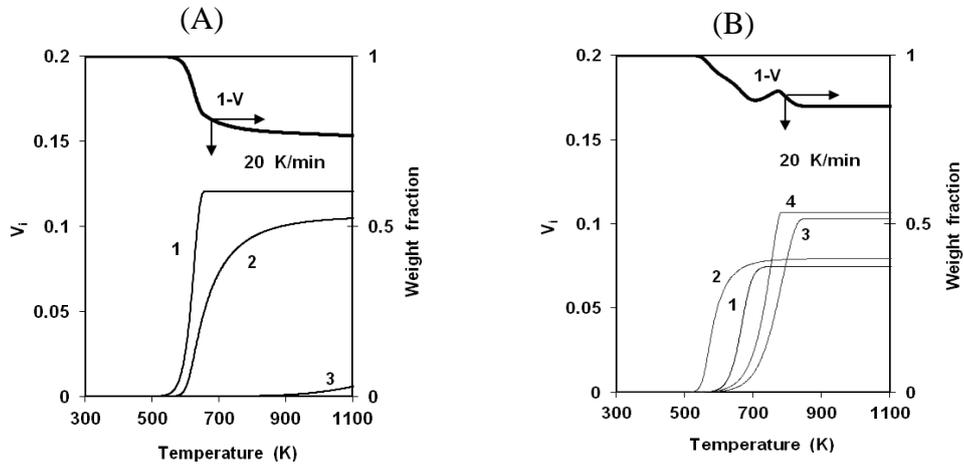
596

597

598 Figure 6. Pyrolysis runs of the non metallic sample: (A) Dynamic experimental runs at
599 three heating rates (the calculated curves overlap the experimental ones) and DTA curve
600 for the run at 20 K min⁻¹. (B) TG and DTG curves (experimental and calculated) at 20 K
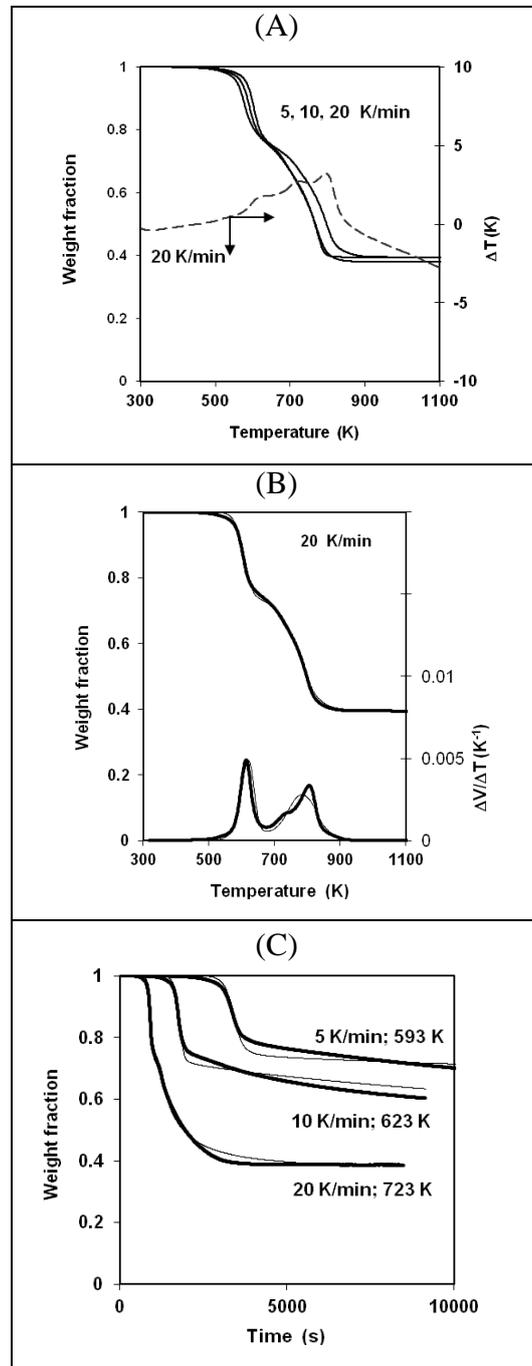601 min⁻¹. (C) Isothermal TG curves (experimental and calculated) at different heating rates.

602
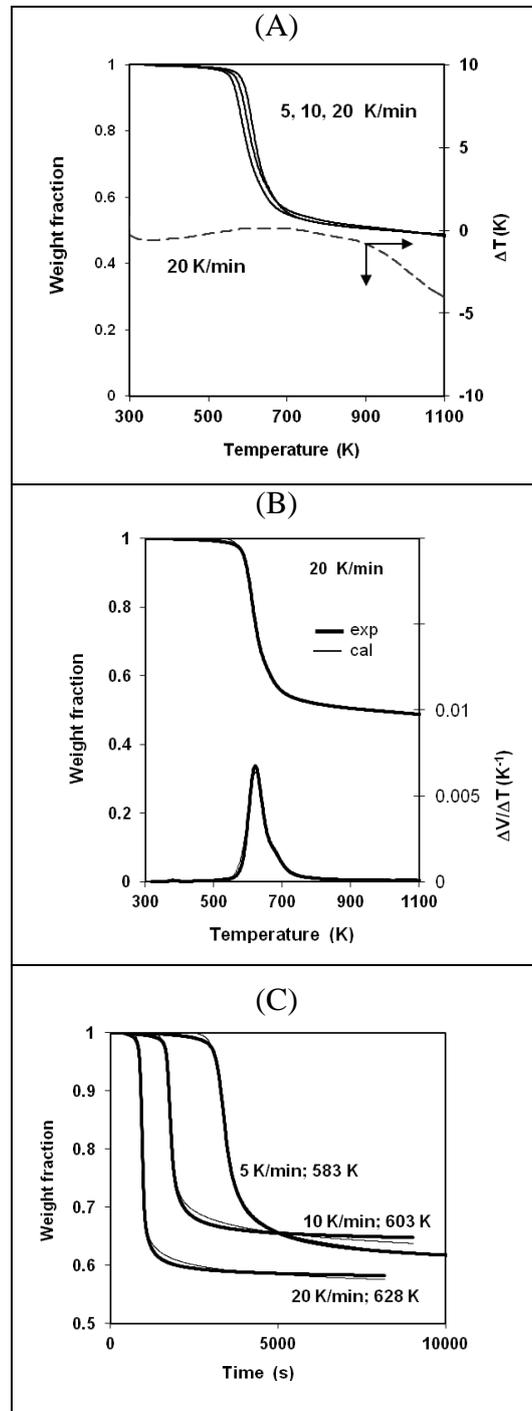
603

604

605 Figure 7. Different combustion runs of non metallic printed circuit boards in $N_2:O_2 =$
606 4:1 atmosphere (experimental and calculated curves): (A) Dynamic TG curves at 5, 10
607 and 20 K min^{-1} and DTA curve for the run at 20 K min^{-1}. (B) TG and DTG run at 20 K
608 min^{-1}. (C) TG isothermal curves at different heating rates.

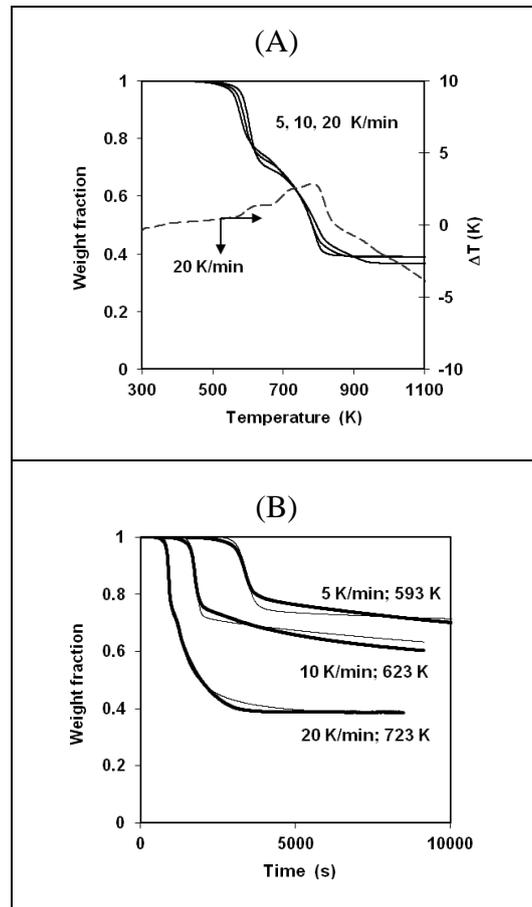609 <mark>Poner curvas experimentales en (A)</mark>

610

611

612   Figure 8. Different combustion runs of non metallic PCB in $N_2:O_2 = 9:1$ atmosphere at

613   5, 10 and 20 K min^{-1} (experimental and calculated curves): (A) Dynamic TG runs. (B)

614   Isothermal TG runs.
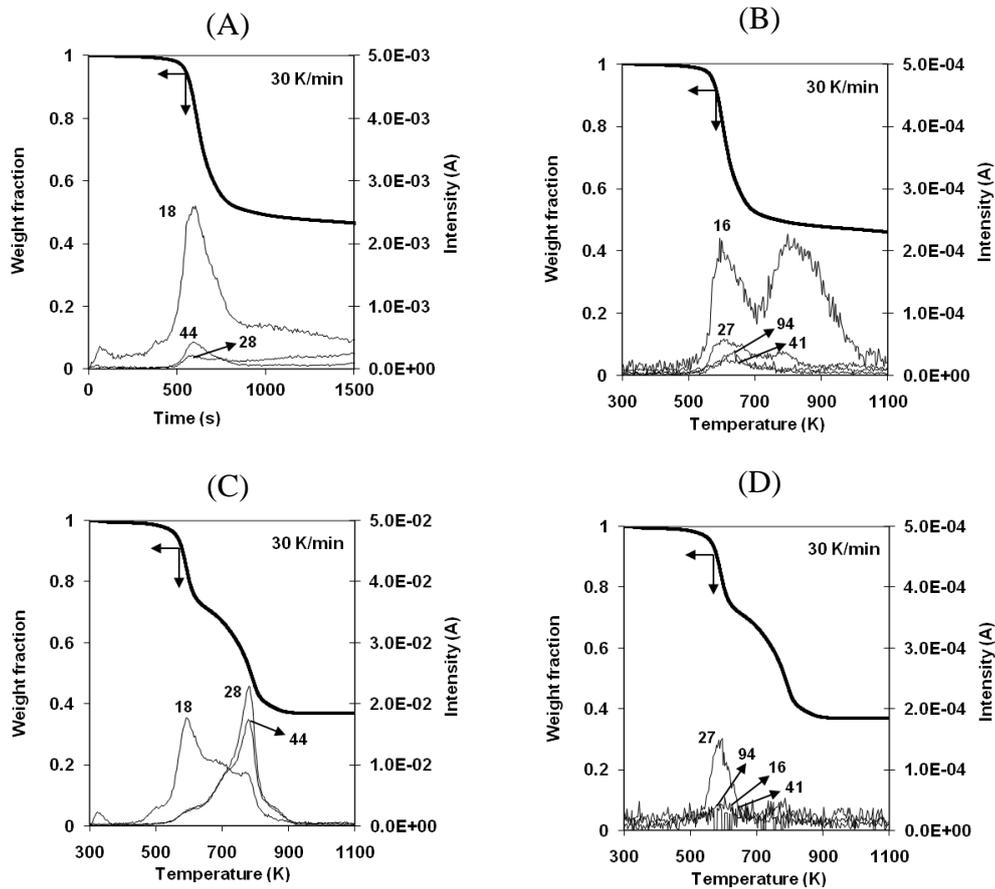
615   Poner curvas experimentales en (A)

616

617

618

619 Figure 9. TG-MS of non metallic printed circuit boards at a heating rate of 30 K min^{-1}:

620 (A) Intensity of ions m/z 18 (water), 28 (CO) and 44 (CO_2) in pyrolysis (He). (B)

621 Intensity of ions m/z 16 (methane), 27 (ethylene), 41 (propylene) and 94 (phenol) in

622 pyrolysis (He). (C) and (D) Intensity of the same ions as (A) and (B) in combustion
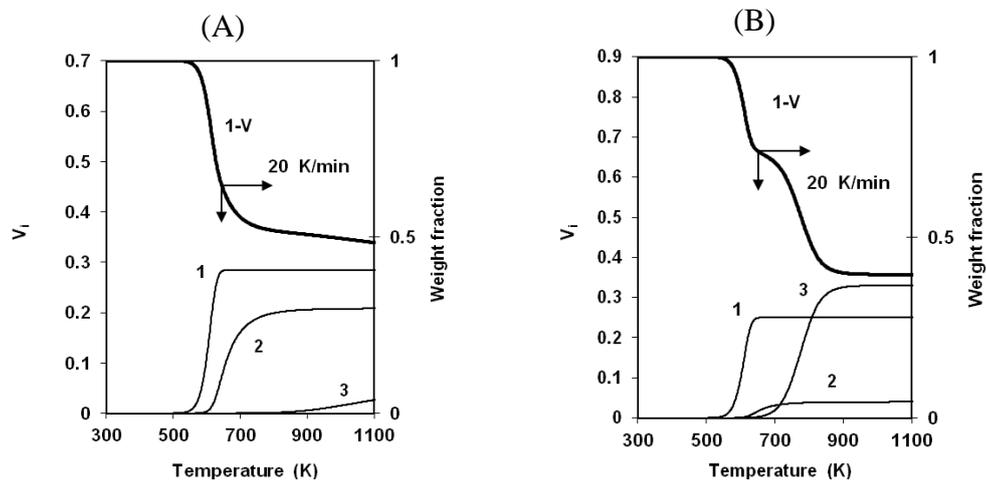
623 (He:O_2 4:1).

624

625

626

627　Figure 10. Evolution of the weight mass and the weight fraction of residues for each

628　reaction, non metallic PCB sample: (A) Pyrolysis TG run. (B) Combustion TG run

629　(N_2:O_2 = 4:1 atmosphere).

630　<mark>CAMBIAR TAMBIÉN PARA QUE BAJEN LOS VOLÁTILES?</mark>

631

632